ELSEVIER

Journal of Power Sources 64 (1997) 39–45

JOURNAL OF POWER SOURCES

Reaction model development for the $Pb/PbSO_4$ system

J.R. Vilche *, F.E. Varela

Instituto de Investigaciones Fisicoquímicas Teóricas y Aplicadas (INIFTA), Facultad de Ciencias Exactas, Universidad Nacional de La Plata, Sucursal 4, C.C.16, 1900 La Plata, Argentina

Abstract

Metal dissolution, active-passive transition and passive layer electroreduction reactions taking place during discharge/charge processes in the lead/sulfuric acid system are discussed on basis of data obtained from steady-state polarizations, potentiostatic pulses, single (STPS) and repetitive (RTPS) triangular potential sweeps, modulated voltammetry, complex voltammetry combined with potentiostatic steps, and electrochemical impedance spectroscopy, using rotating ring (Pb)–disc (Pb) electrode assembly, as well as scanning electron microscopy (SEM). Data analyses derived from transient electrochemical techniques employing parametric identification procedures, non-linear fit routines and computer simulations have been interpreted in terms of appropriate nucleation and growth models for the formation of new phases, in which the characteristics and properties of the compounds generated on the Pb electrode surface exhibit a remarkable dependence on the operational potential.

Keywords: Lead/acid system; Lead electrooxidation; Lead sulfate electroreduction; Lead monooxide electroreduction; Nucleation; Growth mechanisms

1. Introduction

The lead/acid battery is one of the most successful electrochemical energy storage devices, but its design is still open to new developments in order to improve its performance. In this respect, the mechanisms of charge/discharge processes taking place in battery electrodes are of practical interest because of their relevance under operational conditions. Lead electrodes in sulfuric acid electrolytes exhibit a wide variety of phenomena that occur both at the interface and in solid state, and their explanation requires proper use of modern theories of surface electrochemistry as well as those of nucleation and growth of new phases [1–3].

According to Pavlov and co-workers [4,5], the characteristics of passive films formed on lead electrodes in H_2SO_4 solution can be separated into three distinct potential regions: (i) at potentials from -0.95 to -0.30 V (versus Hg/Hg_2SO_4) the passive layer consists of $PbSO_4$ crystals; (ii) the layer produced from -0.30 to 0.95 V is composed of $PbSO_4$ and an inner layer including several basic lead(II) compounds, and (iii) above 0.95 V the α-PbO_2 and β-PbO_2 species become the predominant anodic surface products. The inner layer formed in the intermediate potential range assigned to basic Pb(II)-containing compounds, such as basic lead sulfates, lead hydroxide and lead monoxide, builds up progressively beneath the initially grown $PbSO_4$ as a result of the increasing pH gradient within its porous layered structure.

In previous works [6–17], the kinetics of the electrooxidation of Pb or the electroreduction of surface anodic products formed on Pb electrodes in sulfuric acid solutions at different operational conditions were separately studied. The aim of this paper is to analyse the whole set of experimental data concerning the electrode reactions in the 0–50 °C temperature range in order to postulate a complete scheme of processes involved during the charge/discharge of the lead electrode.

2. Experimental

The experimental setup was described in Refs. [6–17]. High purity polycrystalline Pb in the form of rotating discs or ring (Pb)–disc (Pb) assembly, embedded in polytetrafluoroethylene (PTFE) holders, were used as working electrodes in 5 M H_2SO_4 under nitrogen gas saturation at temperatures covering the 0–50°C range. Potentials were measured and referred to against a Hg/Hg_2SO_4, K_2SO_4 (saturated) reference electrode. Before each electrochemical run, the working electrodes were mechanically polished with 600 and 1200 grade emery papers, thoroughly rinsed with triply distilled water and cathodically polarized in the hydrogen-

* Corresponding author.

PII S0378-7753(96)02498-6

evolution reaction potential region for 5 min, to provide a reproducible electroreduced Pb initial surface.

Runs were performed by using steady-state polarizations, potentiostatic pulses, single (STPS) and repetitive (RTPS) triangular potential sweeps, complex voltammetry combined with potentiostatic steps, and electrochemical impedance spectroscopy (EIS). The different potential routines are illustrated as insets in the figures. Typical perturbing potential programs were the following: (i) triangular potential sweeps between preset cathodic ($E_{s,c}$) and anodic ($E_{s,a}$) switching potentials at a scan rate (ν) comprised in the 7×10^{-5} V $s^{-1} \le \nu \le 0.2$ V s^{-1} range; (ii) combined potential scans and potentiostatic steps, usually two potential steps at E_i and E_f (initial and final potential, respectively), covering different potential regions, in order to modify or reduce the anodic surface products. Data obtained were complemented with scanning electron microscopy (SEM) imaging.

3. Results and discussion

3.1. Electroformation of the anodic layers on Pb during discharge processes

Previous kinetic investigations using linear sweep voltammetry and potential step transients have been interpreted based upon reaction models considering a dissolution/precipitation [3] or a solid-state [18,19] mechanism. The dissolution/precipitation mechanism considers that $PbSO_4$ nuclei are formed in the solution adjacent to the Pb surface, and growth of the three-dimensional $PbSO_4$ layer occurs through Pb electrodissolution and subsequent incorporation of soluble Pb^{2+} species into the growing nuclei. The solid-state mechanism involves $PbSO_4$ nucleation and either a two- or three-dimensional layer growth on the Pb surface [18,19], until this surface becomes mostly covered by $PbSO_4$. The subsequent growth of the $PbSO_4$ crystals involves the transport of Pb^{2+} ions through the $PbSO_4$ layer. It seems that the first mechanism is valid for Pb passivation at relatively low anodic overpotentials, whereas the second predominates at high anodic overpotentials.

In this work, the results of potential sweep and potential step experiments in the Pb electrooxidation potential region are fitted quantitatively to a mechanism consisting of several separate steps, as illustrated in Fig. 1. Thus, the average rate of the overall anodic reaction expressed as $j(t)$, the apparent current density, involves three contributions

$$j(t) = j_g(t) + j_d(t) + j_f(t) \quad (1)$$

which stand for the instantaneous nucleation and two-dimensional growth of the $PbSO_4$ surface film under charge-transfer control, $j_g(t)$, for the Pb electrodissolution from the film free metal surface fraction, $j_d(t)$, and for the Pb dissolution through this initally formed $PbSO_4$ surface film, $j_f(t)$, respectively. The kinetics of the inner $PbSO_4$ layer formation are

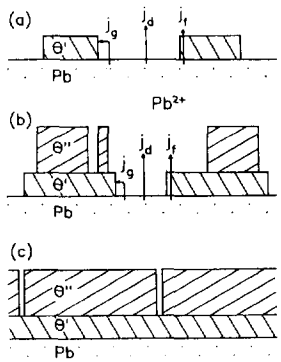

Fig. 1. Scheme of the electrode cross sections during the discharge process. [:·:·] Pb; [\\\] $PbSO_4$ conducting layer (θ'); [///] $PbSO_4$ passivation layer (θ''). The different current contributions are indicated.

governed by instantaneous nucleation followed by two-dimensional growth under charge-transfer control [20]

$$j_g(t) = q_g \frac{d\theta'}{dt}$$

$$= \frac{2\pi n F M_{Su} h_{Su} N_o k^2}{\rho_{Su}} t \exp\left(-\frac{\pi N_o M_{Su}^2 k^2}{\rho_{Su}^2} t^2\right) \quad (2)$$

where θ' is the fractional Pb surface coverage by the inner $PbSO_4$ film (Fig. 1), q_g the apparent charge density of this layer, N_0 the number of nuclei formed instantaneously, k the average film growth rate constant, and M_{Su}, ρ_{Su} and h_{Su} the molecular weight, the density and the average height of the inner $PbSO_4$ layer, respectively.

The dissolution of Pb^{2+} from the bare lead surface should be proportional to the fraction of the surface not covered by the film $(1-\theta')$. Thus

$$j_d(t) = j_d^0(1-\theta') \quad (3)$$

where j_d^0 stands for the Pb^{2+} electrodissolution current for $\theta' = 0$ $(t=0)$.

The above two processes are not sufficient to account for the observed current transients, hence it is proposed that the inner $PbSO_4$ film transmits cations by electromigration in the solid state. These Pb^{2+} cations will enter the electrolyte solution at the outer surface of the film and contribute to the build-up of dissolved Pb^{2+} adjacent to the electrode. The anodic current due to film transmission is proportional to the film coverage θ', but diminishes by the fractional coverage θ'' of a passivating layer of $PbSO_4$ that precipitates on top of the conductive film $(0 \le \theta'' \le \theta')$

$$j_f(t) = 2Fk_f(\theta' - \theta'') \quad (4)$$

Once the concentration of dissolved Pb^{2+} reaches the critical supersaturation limit, precipitation of polycrystalline $PbSO_4$ takes place on the outer surface of the conductive inner film

$$\frac{d\theta''}{dt} = k_p(\theta' - \theta'') \quad (5)$$

This outer passive film does not transmit Pb^{2+} ions and hence electrode passivation occurs.

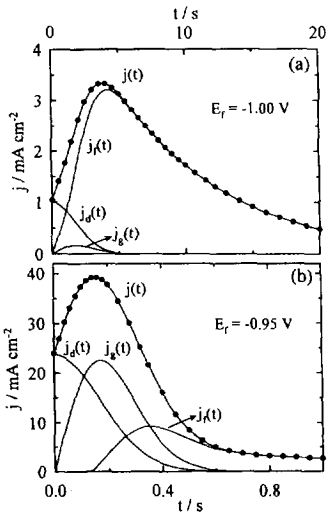

Fig. 2. Comparison of experimental (●) and calculated ($j(t)$) potential step transients. The different anodic current contributions $j_g(t)$, $j_d(t)$, and $j_f(t)$ are indicated. (a) $E_f = -1.00$ V, and (b) $E_f = -0.95$ V.

The above mechanism has been fitted to the experimental data and satisfactory agreement has been obtained for results of potentiostatic steps and potentiodynamic sweeps. Examples of potential step transients are shown in Fig. 2, where the partial currents $j_g(t)$, $j_d(t)$ and $j_f(t)$ and the total current $j(t)$ are compared with experimental data. The results show that at relatively low overpotentials, the dissolution/precipitation mechanism $j_d(t)$ predominates (Fig. 2(a)), whereas the contribution corresponding to the nucleation and growth process $j_g(t)$ becomes important at high anodic overpotentials (Fig. 2(b)). System parameters resulting from parametric identification procedures and non-linear fit routines applied to experimental potentiostatic current transients and voltammograms in order to simulate the electrochemical dynamic responses, yielded values of potential-dependent film thickness and kinetic constants. Particularly, the potential dependence of j_d^0, the current under film free lead surface condition, fulfills a Tafel equation with slope values close to 30 and 120 mV decade^{-1} at low and high overpotentials, respectively. This agrees, in principle, with an initial reversible behaviour of the $Pb \leftrightarrow Pb^{2+} + 2e^-$ reaction, which becomes activation controlled with increasing potential. As one would expect, the value of $(2Fk_f)$, which represents the dissolution of the Pb electrode surface when the conducting $PbSO_4$ layer has already grown, becomes smaller than that obtained through the fitting of j_d^0. Nevertheless, as the cation transfer through the film is a slow process, the contribution $j_f(t)$ explains the slow decay of the current exceeding the current peak and represents the main contribution of $j(t)$ for long times at any anodic potential (Fig. 2(a) and (b)). Voltammogram computer simulation procedures considered that a potential sweep is the sum of an infinite number of potential increments and that between successive increments, the surface coverage of the Pb electrode remains constant [10].

The above results are also consistent with ring–disc electrode data and SEM micrographs. The formation of Pb(II) soluble species during anodization was detected using the ring–disc electrode technique, and it was found that the electroreduction charge corresponding to the Pb^{2+} ions reduced at the ring diminishes as the potential in the disc is shifted positively [8]. These results agree with data shown in Fig. 2(a) and (b). Moreover, SEM micrographs show that the number of $PbSO_4$ crystals increases with the applied potential, in contrast to the average crystal size (Fig. 3). Few and large crystals grow slowly at low potentials under a dissolu-

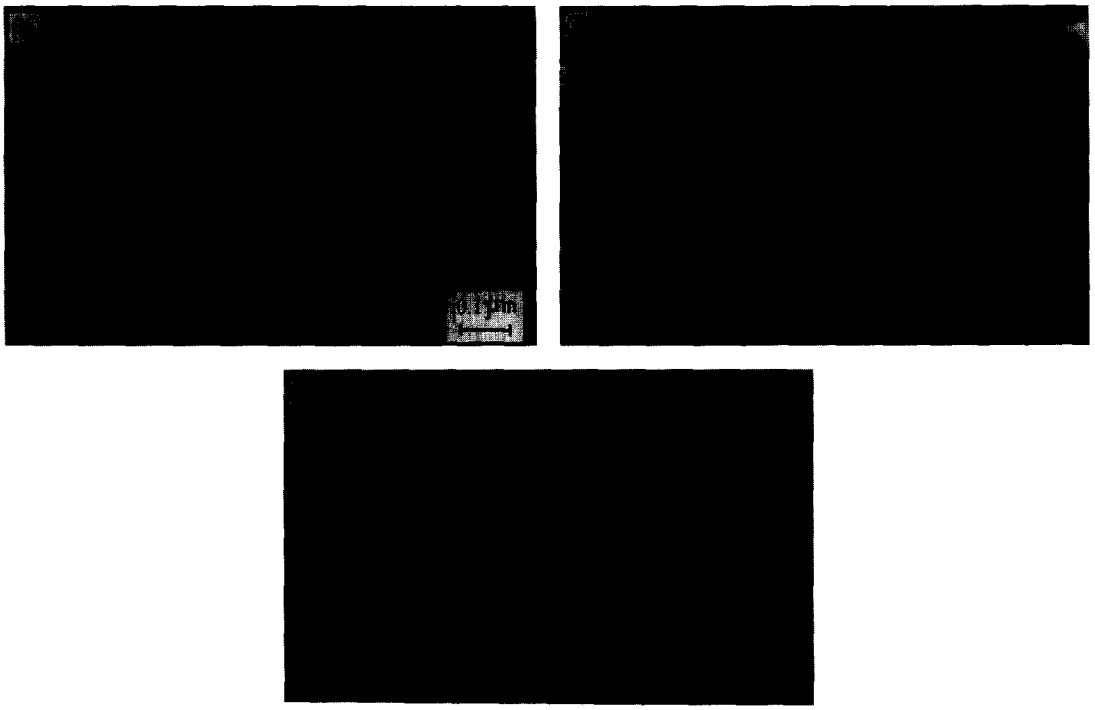

Fig. 3. SEM micrographs of Pb electrodes held at (a) $E_f = -1.020$ V, (b) $E_f = -1.000$ V, and (c) $E_f = -0.975$ V, in 5 M H_2SO_4 solution at 25 °C.

tion/precipitation mechanism, but at higher anodic overpotentials the nucleation and growth process under charge-transfer control, $j_g(t)$, favours the formation of more but smaller $PbSO_4$ crystals.

The concept of the conducting film was first advanced by Pavlov [21] and Pavlov and Popova [22] who admitted that at positive potentials, the inner part of the $PbSO_4$ layer acted simultaneously as a perm-selective membrane for the Pb^{2+} ions, and as a blocking membrane for the access of SO_4^{2-} ions to the interfacial region. This determines the formation of an inner zone with higher concentration of Pb^{2+} ions than that of SO_4^{2-} [21]. Furthermore, as the formation of the passivating layer θ' advances and the pores become narrower (Fig. 1), the Pb^{2+} ion flux is abruptly reduced and, in order to maintain the electrical neutrality, H^+ ions must migrate from the inner zone and the solution within the pores becomes more alkaline. This pH gradient between the solution and the inner zone is maintained as a dynamic equilibrium between an inward diffusional flux of H^+ from the solution, which is 5 M H_2SO_4, and an outward migrational flux of H^+ from the inner zone established by the electric field. The more positive is the applied potential, the higher are the migrational flux and the internal alkalinization. Thus, basic compounds of Pb(II) should be formed at high potentials [6,9,21,22].

Voltammograms of Pb in 5 M H_2SO_4 at $\nu = 0.02$ V s^{-1} run between $E_{s,c} = -1.3$ V and $E_{s,a} = 0.40$ V for different anodization times τ at $E_{s,a}$ are shown in Fig. 4(a) and (b). The positive-going potential sweep exhibits a well-defined anodic current peak (A1) at about -0.96 V corresponding to the electrooxidation of Pb to Pb(II), followed by a wide passive current region (Fig. 4(a)). The potentiodynamic response during the reverse scan exhibits one or two cathodic

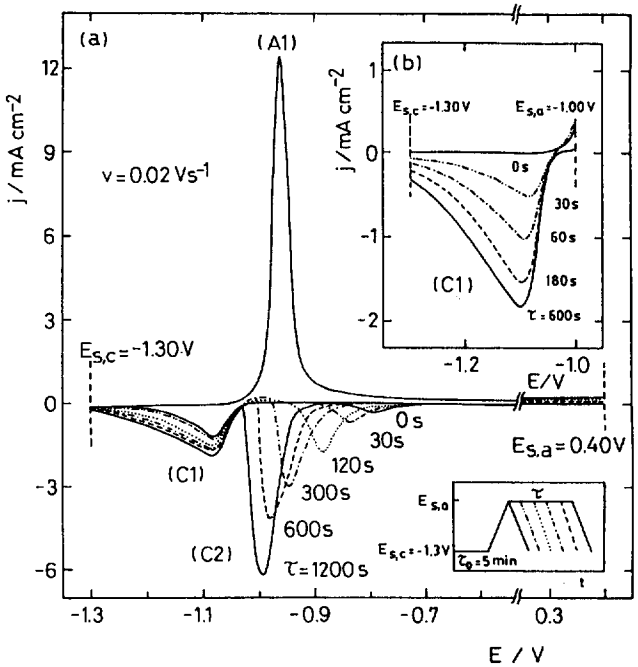

Fig. 4. Voltammograms of Pb in 5 M H_2SO_4 run at $\nu = 0.02$ V s^{-1} between $E_{s,c} = -1.30$ V and (a) $E_{s,a} = 0.40$ V or (b) $E_{s,a} = -1.00$ V, and a potential holding at $E_{s,a}$ for a time τ within the 0 min $\leq \tau \leq$ 20 min range.

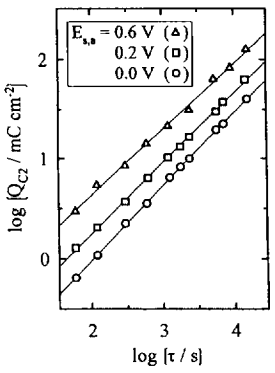

Fig. 5. Dependence of Q_{C2}, at τ, at $E_{s,a}$ from voltammograms run at $\nu = 0.02$ V s^{-1} between $E_{s,c} = -1.30$ V and 0.00 V $\leq E_{s,a} \leq$ 0.60 V.

peaks, depending upon the values of both $E_{s,a}$ and τ. For $E_{s,a} \leq -0.4$ V, only peak C1 located at about -1.10 V is observed (Fig. 4(b)), while for $E_{s,a}$ set at more positive potentials, -0.4 V $< E_{s,a} < 1.0$ V, two cathodic peaks C1 and C2 appear (Fig. 4(a)) [6,9]. The cathodic processes occurring in the potential ranges of peaks C2 and C1 can be associated with the electroreduction of basic Pb(II) compounds (mainly PbO) and $PbSO_4$ layers, respectively [6,9].

The influence of anodizing time τ on the cathodic charge of peaks C1 and C2 can be easily understood, then, within the characteristic features of the model proposed above. At relatively low anodic potentials $E_{s,a}$, the electric field through the anodic layer and the migrational flux of H^+ maintained by it are not high enough to ensure a significative alkalinization. Consequently, the $PbSO_4$ layer continues growing during anodization and the charge of peak C1 increases according to τ (Fig. 4(b)). On the other hand, for higher $E_{s,a}$, H^+ ions become the main current carriers and the charge of peak C2 associated with the electroreduction of PbO, increases with τ while peak C1 remains practically unaltered (Fig. 4(a)). From Fig. 4(a), it is found that the log Q_{C2} (the cathodic charge corresponding to peak C2) increases linearly with log τ according to the following relationship

$$\log Q_{C2} = -0.5 + 0.5 \log \tau \qquad (6)$$

the slope ($\partial \log Q_{C2} / \partial \log \tau$) = 0.5 remains unaltered for $E_{s,a}$ in the 0.0 V $\leq E_{s,a} \leq$ 0.6 V range (Fig. 5). Furthermore, this value agrees with results of Guo et al. [23], who found that the PbO charge passed at constant potential, i.e. Q_{C2}, is proportional to the square root of the polarization time. The rate-determining step of the PbO layer growth is a mass-transfer process: the migration of H^+ ion across the $PbSO_4$ layer and that of OH^- ion across the PbO layer [23].

3.2. Electroreduction of the anodic layers formed on Pb during charge processes

In the passive potential range, a PbO layer builds up progressively beneath the $PbSO_4$ porous layer initially produced. The comparison between experimental results and simulated data suggests that during Pb electrode discharge, the electrolyte penetration in the pores of the $PbSO_4$ crystal structure

ensures the current flow through the $PbSO_4$ layer, which transforms gradually into a semipermeable membrane hindering the diffusion of SO_4^{2-} ions and causing an increase of the Pb^{2+} ion concentration in the inner zone of the passive layer. The formation of PbO arises as a consequence of the local alkalinization at the $Pb/PbSO_4$ interface. Hence, local pH changes due to different permeability of the $PbSO_4$ layer between different regions determine variations in the PbO layer thickness across the electrode surface.

The impedance diagrams recorded in the potential range where a composite Pb(II)–containing sulfate/oxide passive layer is produced, exhibit a complex frequency response, where the insulating behaviour of the $PbSO_4$ layer contribution appears at the lower frequencies. The analysis of high frequency data indicated that the inner barrier PbO layer behaves as a semiconductor [9]. The charge-carrier concentration decreases slightly as a passive film formation potential is fixed more positively. A Warburg-like diffusion component was detected in the intermediate frequency region and it can be attributed to the H^+ ion transport process due to the increasing alkalinity of the Pb/film interface as the PbO layer is formed in the inner portion of the surface film [9].

In spite of this complex surface-layer structure, the electroreduction of the PbO and $PbSO_4$ layers can be studied using conventional planar electrode models provided that simulation data prove to be autoconsistent. Let us consider the PbO electroreduction. Dynamic system analysis applied to the set of data resulting from combined voltammetry and potentiostatic current transient techniques allows us to explain the kinetics of the electroreduction of PbO layers, mainly in terms of a progressive nucleation and a three-dimensional growth mechanism under charge-transfer control whereas in the initial short time range a process under H^+ ion diffusion control has been detected [6,14,15]. The initial electroreduction process is related to the electroreduction of Pb(II) ions controlled by the diffusion of H^+ from the outer $PbSO_4$ layer to the inner passive film. Rate constants of the main current contribution fit an Arrhenius-type behaviour [14]. Results suggest that the thermal increase in the crystal growth perpendicular to the plane surface is about twice that in the parallel direction. Furthermore, the activation enthalpy includes two contributions, one related to an ordinary chemical reaction and the other to the reversible electrochemical reaction taking place at the inner portion of the passive film structure [14].

Potentiostatic cathodic current transients corresponding to the PbO electroreduction process at $E_f = -0.90$ V after a potential step at $E_{s,a} = E_i = 0.40$ V for τ in the range 30 s $\leq \tau \leq$ 30 min are shown in Fig. 6. According to the kinetic model above proposed, these transients can be appropriately described by the expression

$$j(t) = zFk_{\perp}\theta_i(t)[1-\theta_i(t)] + P_{D1}\exp(-P_{D2}t) \quad (7)$$

with

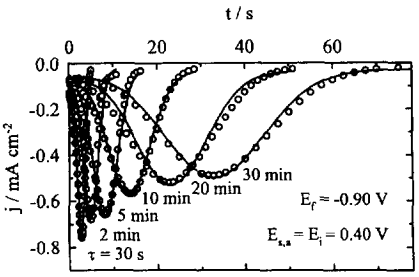

Fig. 6. Fitting of current transient data recorded at $E_f = -0.90$ V after a potential holding at $E_i = E_{s,a} = 0.40$ V during different τ in the 30 s $\leq \tau \leq$ 30 min range, according to Eq. (7) (full traces).

$$\theta_i(t) = \exp\left(-\frac{\pi M_{Ox}^2 A k_{\parallel}^2}{3\rho_{Ox}^2} t^3\right) \quad (8)$$

where $\theta_i(t)$ is the coverage by the PbO species at the inner surface layer, $k_{\perp}$ and $k_{\parallel}$ denote the rate constants describing crystal growth perpendicular and parallel to the plane surface electrode, respectively, A is the nucleation rate constant, ρ_{Ox} the density of the layer and M_{Ox} the PbO molecular weight. In Eq. (7), the main term corresponds to the progressive nucleation and the three-dimensional growth under a charge-transfer control process [24], whereas the second term, which predominates only at very short times, is related to the instantaneous nucleation and a two-dimensional growth process under diffusion control (P_{D1} and P_{D2}) [14,15].

Fig. 6 also illustrates a good agreement between the experimental and calculated data. The potential E_f was chosen to allow the separation of the electroreduction process of the inner PbO layer from that corresponding to the $PbSO_4$ species, which takes place when $E_f \leq -1.05$ V. It is important to mention that the electroreduction charge of the current transients increases with τ according to Eq. (6), determined from voltammectric results, but for each τ it remains unaltered for E_f varying in the whole potential range of the voltammetric peak C2, i.e. $-0.82 \leq E_f \leq -1.02$ V. The values of the model parameters for different E_f and τ, corresponding to $E_i = 0.40$ V, can be obtained from the following relationships:

$$\log k_{\perp} = -12.19 - 8.34E_f - 0.101 \log \tau \quad (9)$$

$$\log(Ak_{\parallel}^2/\rho_{Ox}^2) = -25.94 - 25.10E_f - 1.82 \log \tau \quad (10)$$

These relationships yield slopes $[(\partial E_f/\partial \log k_{\perp})]_{\tau} = -0.120$ V/decade and $[\partial E_f/\partial \log(Ak_{\parallel}^2/\rho_{Ox}^2)]_{\tau} = 0.040$ V/decade, with values in agreement with those reported previously from data obtained at shorter anodization times during Pb discharge, e.g., thinner passive layers [14,15].

Furthermore, the charge density comprised in the case of the instantaneous nucleation and two-dimensional growth process under diffusion control is given by the P_{D1}/P_{D2} ratio [6]. This charge density, which is associated with the small current contribution described for the second term in Eq. (7), seems to be practically constant in the whole E_f range covered in this work, and it involves less than 10% of the whole electroreduction charge. During the previous anodic polarization of the Pb electrode in the discharge process, the local pH increases due to the decrease of the concentration of

SO_4^{2-} and the increase of the concentration of Pb^{2+} in the inner zone of the passive film. When polarization turns into cathodic values during the charge stage, the Pb^{2+} concentration decreases abruptly and, in order to maintain the electroneutrality of the solution in the pores, H^+ ions migrate from the solution into the pore and combine with the OH^- liberated from the PbO electroreduction. Thus, the initial electroreduction current decay can be related to the electroreduction of Pb(II) ions controlled by the diffusion of OH^- to the solution or H^+ to the inner layer of the passive film.

In order to achieve a simulation of the electrode response to a cathodic potential sweep, it is necessary to describe the current density j and the surface coverage θ_i in terms of the dependent variables E and t for any given transient. As the second term of the current density in Eq. (7) makes only a small contribution to the whole faradaic charge, for the sake of simplicity it is neglected in the voltammetric simulations. Thus, the use of Eqs. (8)–(10) combined with the first term of Eq. (7) allows the complete description of the voltammograms. The method has been described in detail in Refs. [10,15,25]. Simulated cathodic voltammograms for different anodization times τ at $E_{s,a}$ shown in Fig. 7 exhibit identical trends to the experimental ones. The apparent cathodic charge density of the simulated voltammograms increases according to τ following Eq. (6) closely. As the first term in Eq. (7) comprises the main current contribution, the cathodic charge involved in the electroreduction of PbO layers can be approximated by [6]

$$Q_{PbO} \approx 0.18(zFk_{\perp})\left(\frac{\pi M_{Ox}^2 A k_{\parallel}^2}{3\rho_{Ox}^2}\right)^{-1/3} \quad (11)$$

and

$$\log Q_{PbO} \approx \log 0.18 + \log(zFk_{\perp}) - (1/3)\log\left(\frac{\pi M_{Ox}^2 A k_{\parallel}^2}{3\rho_{Ox}^2}\right) \quad (12)$$

Thus, the parametric functionalities of data given by Eqs. (9) and (10) approach the values predicted by the well-established reaction model, according to Eqs. (6) and (12).

Combined voltammetry and potentiostatic current transient techniques have been also employed to study the electroreduction processes of the anodically fomed $PbSO_4$ layers [6,13]. The kinetic data suggests that the electroreduction of the $PbSO_4$ layer involves mainly an instantaneous nucleation and three-dimensional growth mechanism under diffusion control. In the short-time range, after correction for the electrical double-layer discharge the initial falling current transients obey an instantaneous nucleation and two-dimensional growth under diffusion control. The latter can be associated with the diffusion-controlled reversible electroreduction of Pb(II) ions, whose concentration under critical supersaturation condition at 25 °C seems to attain a value of about 2×10^{-6} mol cm^{-3}, which is consistent with a diffusion coefficient close to 10^{-6} cm^2 s^{-1}.

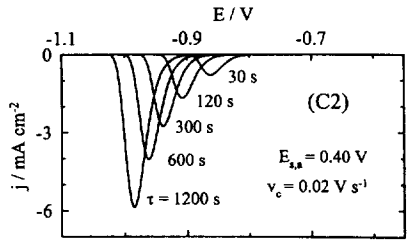

Fig. 7. Influence of τ on the simulated voltammetric data.

The experimental results for the electroreduction of PbO and $PbSO_4$ layers at temperatures in the 0–50 °C range, varying E_i and E_f at convenience, are in accordance with the above proposed kinetic models. The kinetic study was conducted at temperatures up to 50 °C taking into account that at about 60 °C a degradation in operation life of automotive batteries is usually observed [2,3]. Potentiostatic current transients corresponding to the electroreduction of $PbSO_4$ layers formed at different temperatures by a linear potential scan at $\nu_a = 0.02$ V s^{-1} between $E_{s,c} = -1.3$ V and $E_{s,a} = E_i = -1.0$ V, i.e. in the peak A1 potential range, are shown in Fig. 8. The electroreduction process at E_f was preceded by a potential hold during $\tau = 3$ min at E_i, which is remarkably more negatively located than the potential region of PbO layer formation. These experimental current transients can be satisfactorily reproduced (full traces in Fig. 8) through the expression [6,13]

$$j(t) = zFD_j^{1/2}\Delta c_j \pi^{-1/2} t^{-1/2}[1 - \exp(-N_0 \pi K_j D_j t)] + zFD_i^{1/2}\Delta c_i \pi^{-1/2} t^{-1/2} \quad (13)$$

where K_j denotes a proportionality constant, $K_j = (8\pi\Delta c_j M_{su}\rho_{Su}^{-1})^{1/2}$, D_j and Δc_j are the diffusion coefficient and the concentration difference of the mobile species j inside the solution in pores of the surface films, N_0 are the nuclei instantaneously formed, M_{Su} is the molecular weight of $PbSO_4$ and ρ_{Su} is the density of the surface layer. The main contribution implies current control by diffusion of lead ions in the film, the calculated value of $(D_j^{1/2}\Delta c_j)$ from voltammograms is in accordance with that derived from current transient fit parameters, the diffusion coefficient at 25 °C being in this case about $D_j \approx 3\times10^{-11}$ cm^2 s^{-1} and the nuclei instantaneously formed about 8×10^{10} cm^{-2}.

The influence of the temperature on the set of adjusted parameters furnishes additional data related to the energies of the involved processes and allows a new insight about the influence of temperature on the performance of the lead/acid

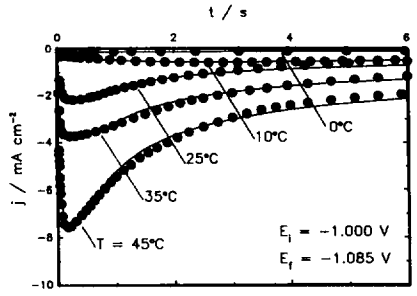

Fig. 8. Fitting of current transient data recorded at different temperatures and $E_f = -1.085$ V after a potential holding at $E_i = -1.000$ V during $\tau = 3$ min, according to Eq. (13) (full traces).

battery. Let us consider the following possible consecutive reactions involved in the Pb(II)–sulfate layer electroreduction mechanism

$$PbSO_4 + H_3O^+ \rightarrow Pb^{2+} + HSO_4^- + H_2O \quad (14a)$$

$$Pb^{2+} + 2e^- \rightarrow Pb \quad (14b)$$

Eq. (14) implies a phase-transition process, whose kinetics can be interpreted by a nuclation and three-dimensional growth mechanism under diffusion control, so that H_3O^+/HSO_4^- or Pb^{2+} ions migrate alternately through the $PbSO_4$ layer, and in a fast electron-transfer step (Eq. (14b)) the Pb^{2+} ions are electroreduced on the surface. The calculated activation enthalpy of the diffusion-controlling step yields $\Delta H^*_{Dj} = 95.7$ kJ mol^{-1}. This value is in close agreement with that found by Valeriote and Gallop [26] during the oxidation of anodic films on lead in sulfuric acid solutions at low temperatures, where the rate-limiting diffusion of ions may be controlled by an activation process involving the partial dehydration of the diffusing ion and/or desorption of interfacial water. On the other hand, for the process occurring during the initial falling current transient, ΔH^*_{Di} close to 40.2 kJ mol^{-1} was obtained. This valued was found to be larger than that expected for an ion diffusion process in solution, but it gives support to the conclusion that can be related to diffusion-controlled electroreduction of Pb(II) ions from the supersaturated solution within the pores located between the $PbSO_4$ crystals.

4. Conclusions

The kinetics of the Pb/Pb(II) charge/discharge electrochemical reactions in sulfuric acid solutions were investigated using different potential perturbing techniques. Results showed that both the electrooxidation of Pb and the subsequent electroreduction of the surface anodic products corresponded to highly irreversible processes. Thus, the electrochemical process related to the discharge of the Pb electrode can be explained through a complex mechanism that includes a nucleation and two-dimensional growth under charge-transfer process in parallel with a dissolution/precipitation one. On the other hand, the electroreduction of the $PbSO_4$ layer during the charge process involves mainly an instantaneous nucleation and three-dimensional growth mechanism under diffusion control.

Furthermore, as the internal alkalization of the $PbSO_4$ layer promotes the formation of basic Pb(II) compounds, it was established that the rate-determining step of the slow PbO layer growth is a mass-transfer process: the migration of H^+/OH^- ions through the anodic layer. During the electroreduction of the PbO film, however, the H^+/OH^- diffusion-controlled process represents less than 10% of the whole electroreduction charge. Likewise, the main electroreduction contribution corresponds to a three-dimensional progressive nucleation with charge-transfer controlled growth process.

Acknowledgements

This research project was financially supported by the 'Consejo Nacional de Investigaciones Científicas y Técnicas', the 'Comisión de Investigaciones Científicas de la Provincia de Buenos Aires', and the 'Fundación Antorchas'. Part of the equipment used in the present work was provided by the DAAD and the 'Alexander-von-Humboldt Stiftung'.

References

[1] T.F. Sharpe, in A.J. Bard (ed.), *Encyclopedia of Electrochemistry of the Elements*, Vol. 1, Marcel Dekker, New York, 1973, p. 235.
[2] H. Bode, *Lead–Acid Batteries*, Wiley, New York, 1977.
[3] K.R. Bullock and D. Pavlov (eds.), *Advances in Lead–Acid Batteries*, The Electrochemical Society, Pennington, NJ, USA, 1984.
[4] D. Pavlov, C.N. Poulieff, E. Klaja and N. Iordanov, *J. Electrochem. Soc., 116* (1969) 316.
[5] D. Pavlov, S. Zanova and G. Papazov, *J. Electrochem. Soc., 124* (1977) 1522.
[6] F.E. Varela, L.M. Gassa and J.R. Vilche, *Electrochim. Acta, 37* (1992) 1119.
[7] F.E. Varela, L.M. Gassa and J.R. Vilche, *J. Braz. Chem. Soc., 3* (1992) 43.
[8] F.E. Varela, M.E. Vela, J.R. Vilche and A.J. Arvia, *Electrochim. Acta, 38* (1993) 1513.
[9] F.E. Varela, L.M. Gassa and J.R. Vilche, *J. Electroanal. Chem., 353* (1993) 147.
[10] F.E. Varela, J.R. Vilche and A.J. Arvia, *Electrochim. Acta, 39* (1994) 401.
[11] E.N. Codaro, F.E. Varela and J.R. Vilche, *J. Braz. Chem. Soc., 5* (1994) 143.
[12] F.E. Varela, E.N. Codaro and J.R. Vilche, *J. Braz. Chem. Soc., 5* (1994) 149.
[13] F.E. Varela, L.M. Gassa and J.R. Vilche, *J. Appl. Electrochem., 25* (1995) 358.
[14] F.E. Varela, L.M. Gassa and J.R. Vilche, *J. Appl. Electrochem., 25* (1995) 364.
[15] F.E. Varela, E.N. Codaro and J.R. Vilche, *Electrochim. Acta, 40* (1995) 1183.
[16] F.E. Varela, E.N. Codaro, L.M. Gassa and J.R. Vilche, *Proc. Int. Symp. Electrochemical Science and Technology*, The Hong Kong University, 1995, L11/1–16.
[17] E.N. Codaro and J.R. Vilche, *Electrochim. Acta, 42* (1997) 549.
[18] G. Archdale and J.A. Harrison, *J. Electroanal. Chem., 34* (1972) 21; *39* (1972) 357.
[19] N.A. Hampson and J.B. Lakeman, *J. Electroanal. Chem., 107* (1980) 177.
[20] J.A. Harrison and H.R. Thirsk, in A.J. Bard (ed.), *Advances in Electroanalytical Chemistry*, Vol. 5, Marcel Dekker, New York, 1971, pp. 67–148.
[21] D. Pavlov, *Electrochim. Acta, 13* (1968) 2051; *23* (1978) 845.
[22] D. Pavlov and R. Popova, *Electrochim. Acta, 15* (1970) 1483.
[23] Y. Guo, S. Hua, H. Xu and Y. Yang, *J. Electrochem. Soc., 143* (1996) 1157.
[24] R.D. Armstrong, M. Fleischmann and H.R. Thirsk, *J. Electroanal. Chem., 11* (1966) 208.
[25] R.G. Barradas, F.C. Benson and S. Fletcher, *J. Electroanal. Chem., 80* (1977) 305.
[26] E.M. Valeriote and L.D. Gallop, *J. Electrochem. Soc., 124* (1977) 370, 380.